Effect of Nd Additions on Extrusion Texture Development and on Slip Activity in a Mg-Mn Alloy

PALOMA HIDALGO-MANRIQUE, S.B. YI, J. BOHLEN, D. LETZIG, and M.T. PÉREZ-PRADO

Two Mg-1 wt pct Mn alloys containing 0.5 wt pct and 1 wt pct Nd have been processed by indirect extrusion at temperatures ranging from 548 K (275 °C) to 633 K (360 °C) and speeds between 2.8 and 11 mm/s. The microstructure and the texture of the extruded bars were analyzed in order to understand the effect of the processing parameters and of the rare-earth (RE) alloying additions on the texture development. Increasing the Nd content results in weak textures in which the predominant orientations are a function of the extrusion conditions. This may be explained by the occurrence of particle pinning of grain boundaries and by the nucleation of grains with a wider range of orientations. Mechanical tests were carried out in tension and in compression in all the processed samples at 10^{-3} s^{-1} and room temperature. It was found that larger RE amounts give rise to the disappearance of the yield asymmetry and to an anomalously high activity of tensile twinning, especially at the lowest extrusion temperatures. This has been attributed to an increase of the critical resolved shear stress of basal slip due to the presence of Mg$_3$Nd coherent and semi-coherent intermetallic prismatic plates.

I. INTRODUCTION

MAGNESIUM (Mg) and its alloys are promising structural materials due to their weight-saving possibilities. However, wrought Mg products are typically characterized by an excessive directionality of the mechanical properties,[1] which restricts many of their potential applications. As such, the mechanical properties of Mg alloy extrusions are affected by undesirable yield asymmetry, which results in limited formability and unusual bending characteristics, such as failure initiation on the compressive side of bent parts.[2] Typically, the compressive yield stress can be as little as half the tensile yield stress when tested along the extrusion direction (ED).[1]

The yield asymmetry of extruded round bars is due to the formation of the well-known prismatic $\langle 10\bar{1}0 \rangle$ fiber texture or the $\langle 10\bar{1}0 \rangle$–$\langle 11\bar{2}0 \rangle$ double fiber texture, with the {0001} basal planes being parallel to the ED.[3] Due to the polar nature of mechanical twinning,[4] extension twinning along the {10$\bar{1}$2} planes is active only when the deformation conditions are such that an extension along the c-axis takes place.[5] Accordingly, a strong typical extrusion texture favors twinning in compression, but not in tension along the ED, which results in the above-described asymmetry between the tensile and the compressive yield stresses.

One way of modifying the deformation behavior of the Mg extrusions, and in particular the twinning response, is to alter the extrusion texture by alloying. It has been shown that the addition of certain rare-earth (RE) elements including yttrium (Y), even in dilute concentrations, promotes weaker extrusion textures or broader distributions of the basal planes toward the ED, leading to reduced yield asymmetries.[6–8] It is currently assumed that the texture weakening in the RE-containing Mg alloys is primarily a recrystallization phenomenon rather than a direct effect on the deformation texture. However, the specific mechanisms are currently under discussion. It has been suggested that the weakened texture can be attributed to particle-stimulation nucleation (PSN).[6] Alternatively, weakened textures have been associated to nucleation at deformation heterogeneities, such as shear bands.[9] It has also been proposed that RE elements have an effect on boundary mobilities leading to oriented growth.[7] Such effects may be related to a form of particle pinning or solute drag that alters orientation relationships for high boundary mobility. In this way, unusual orientations would develop certain growth advantages leading to weaker and nearly random textures.

Mg-Mn-based alloys, usually containing relatively high amounts of manganese (1–2 wt pct Mn), have good extrudability and weldability combined with medium strength.[10] Moreover, Mn removes elements with a deleterious effect on corrosion, like iron (Fe) and silicon (Si), and promotes the formation of relatively harmless intermetallic compounds, conferring the Mg-Mn alloys a good corrosion resistance.[1] Thus, the latter are good candidates for base materials in studies aiming to enhance the formability of wrought Mg alloys. Recently, single additions of RE elements such as cerium (Ce),

PALOMA HIDALGO-MANRIQUE, Research Associate, and M.T. PÉREZ-PRADO, Senior Researcher, are with the IMDEA Materials Institute, C/Eric Kandel 2, 28906 Getafe, Madrid, Spain. Contact e-mail: paloma.hidalgo@imdea.org S.B. YI and J. BOHLEN, Scientists, and D. LETZIG, Head of Department, are with the Magnesium Wrought Alloys Department, Magnesium Innovation Centre MagIC, Helmholtz-Zentrum Geesthacht, Max-Planck-Strasse 1, 21502 Geesthacht, Germany.

yttrium (Y), and neodymium (Nd) have been made to Mg-Mn alloys in earlier work[8] in order to investigate their influence on the microstructure and texture formed during indirect extrusion and the resulting mechanical properties. Nd was found to be a much stronger texture modifier than Ce or Y.

In the present study, extrusion experiments were carried out at different temperatures using several extrusion speeds on two variations of the M1 alloy (nominally Mg-1 wt pct Mn) including 0.5 and 1 wt pct of Nd. The microstructure, texture and mechanical behavior of the processed samples were then examined thoroughly. The aim of the work was, first, to investigate the effect of both the processing parameters as well as the RE additions in the texture and microstructure development during extrusion and, second, to relate this to the mechanical asymmetry and to the incidence of various recrystallization and deformation mechanisms.

II. EXPERIMENTAL PROCEDURE

The materials investigated are two extruded Mg-1 wt pct Mn alloys, with up to 1 wt pct Mn in solid solution and containing 0.5 and 1 wt pct Nd. These alloys are termed MN10 and MN11, respectively. The materials were first gravity cast in order to produce billets for extrusion, which were machined up to a diameter of 93 mm. Second, and before extrusion, the billets were homogenized at 623 K (350 °C) for 15 hours. Then, indirect extrusion was performed under 13 different conditions, summarized in Table I, to produce round bars of 17 mm in diameter, which corresponds to an extrusion ratio of 1:30. The nomenclature of the 13 extruded bars is also included in this table.

The microstructure of all the samples was characterized by optical microscopy (OM) in an Olympus BX-51 microscope. The OM analysis was performed on regions located at the center of the extruded bars in sections parallel to the ED. The grain size was measured by the linear intercept method in those optical micrographs taken from the most representative areas of the samples. Surface preparation for OM consisted of grinding with increasingly finer SiC papers and several diamond

polishing steps. The specimens prepared were additionally chemically etched in a solution based on picric and acetic acids.

The macrotexture of all the specimens was examined by X-ray diffraction (XRD). The (0001), (10$\bar{1}$0), (10$\bar{1}$1), (10$\bar{1}$2), (10$\bar{1}$3), and (11$\bar{2}$0) pole figures were measured using Cu K$_\alpha$ radiation in an Xpert-Pro Panalytical diffractometer furnished with a PW3050/60 goniometer. From these experimental data, the ODF and the calculated pole figures were obtained using the MATLAB toolbox MTEX. The inverse pole figures were then derived from the calculated direct pole figures. XRD analysis was also performed on some extrusions to characterize the different phases present using the Bragg–Brentano method. The 2θ angle ranged from 10 to 130 deg with a step of 0.04 deg. The XRD analysis was performed on regions located at the center of the extruded bars in sections perpendicular to the ED. Sample preparation for XRD analysis was the same as that described above for OM, except for the last etching step.

Examination of the precipitates present was carried out in an EVO MA15 scanning electron microscope (SEM). Quantitative analysis of the chemical compositions of the phases in the examined samples was conducted using Oxford energy dispersive X-ray spectrometer (EDS). Data acquisition and analysis were performed using the commercial INCA 330 software. The SEM analysis was performed on regions located at the center of the extruded bars in sections perpendicular to the ED. Samples for SEM investigations were also ground with SiC papers and polished using diamond paste.

Uniaxial tension and compression tests along the ED of the samples machined from all the extruded bars were carried out at room temperature in a servo-electric (100 KN) Instron machine at an initial strain rate of 10^{-3} s^{-1}. Two tests were performed for each condition, as the mechanical behavior was observed to be highly reproducible. The tensile specimens had cylindrical geometry with a gage section 4 mm in diameter and 12 mm in length and the compressive specimens had also cylindrical geometry with 3 mm diameter and 4.5 mm height. The true stress (σ)–true strain (ε) curves were calculated using standard expressions. From the curves, the yield stress (σ_y) was estimated as the true stress at 0.2 pct strain. In addition, the slope of the σ–ε curves at each strain level, *i.e.*, the work hardening rate ($\theta = d\sigma/d\varepsilon$), was calculated.

Table I. Composition, Extrusion Parameters, and Nomenclature of the 13 Extruded Bars Investigated

Alloy	Temperature	Speed (mm/s)	Nomenclature
MN10	573 K (300 °C)	2.8	MN10-300α
MN10	573 K (300 °C)	5.5	MN10-300β
MN10	573 K (300 °C)	8.3	MN10-300γ
MN10	633 K (360 °C)	2.8	MN10-360α
MN10	633 K (360 °C)	5.5	MN10-360β
MN10	633 K (360 °C)	11	MN10-360γ
MN11	548 K (275 °C)	2.8	MN11-275α
MN11	548 K (275 °C)	5.5	MN11-275β
MN11	548 K (275 °C)	8.3	MN11-275γ
MN11	573 K (300 °C)	5.5	MN11-300β
MN11	623 K (350 °C)	2.8	MN11-350α
MN11	623 K (350 °C)	5.5	MN11-350β
MN11	623 K (350 °C)	11	MN11-350γ

III. RESULTS

Figures 1 and 2 illustrate the microstructure corresponding to longitudinal sections of the MN10 and MN11 extruded rods, respectively, processed at different temperatures and extrusion speeds. The average grain size has been added as an inset to each micrograph. In general, all the extrusions exhibit a fully recrystallized microstructure, comprising fine equiaxed grains with a homogeneous size, the average value of which ranges from 11 to 22 μm. Large insoluble constituent intermetallic particles that consist of
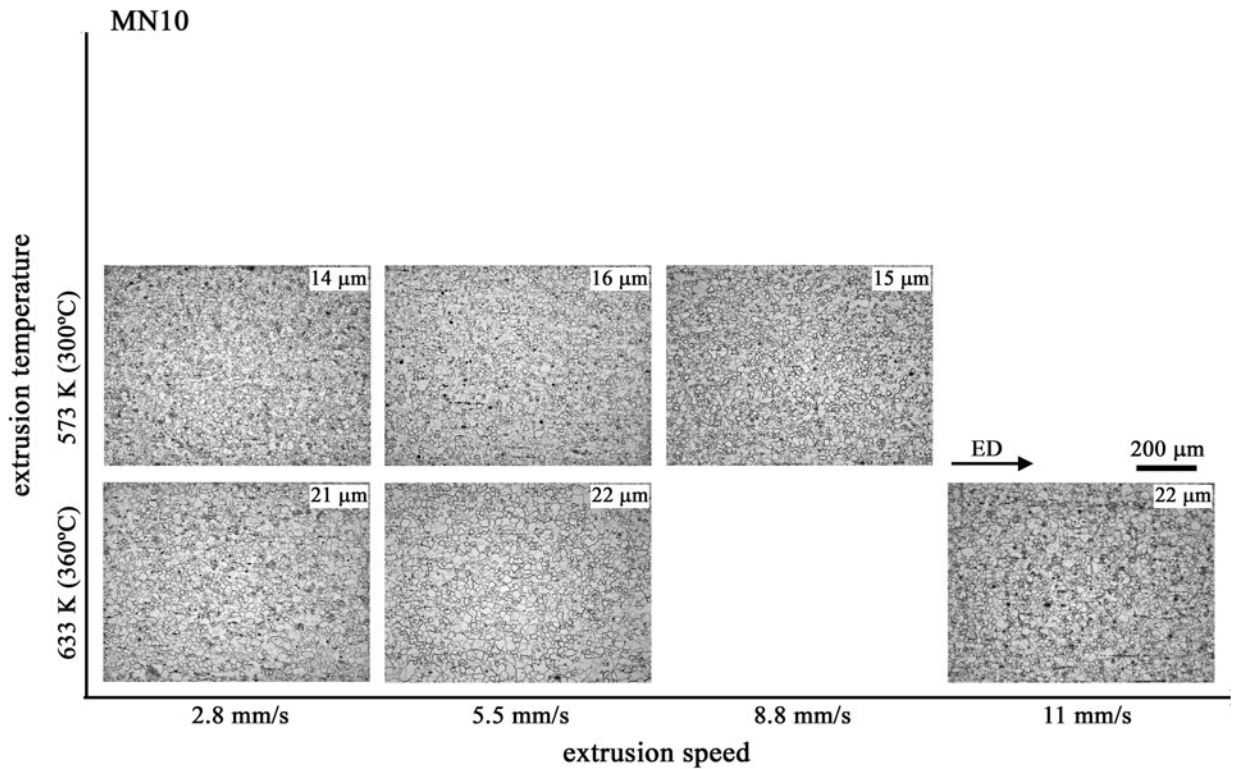
Fig. 1—Optical micrographs from the longitudinal section of the MN10 extrusion bars. The average grain size of each extrusion is also included.
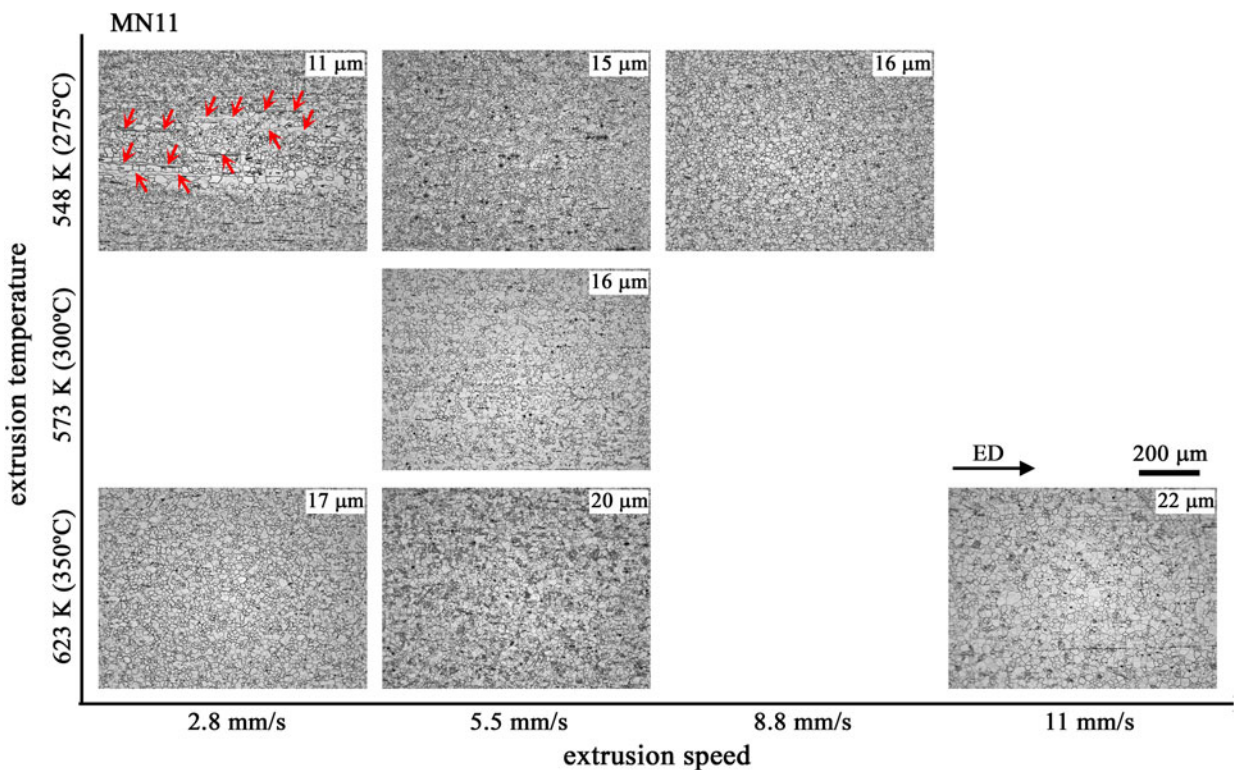

Fig. 2—Optical micrographs from the longitudinal section of the MN11 extrusion bars. The average grain size of each extrusion is also included. The *red arrows* highlight the deformed grains (Color figure online).

Fe and Mn,[11] often aligned along the ED, are also apparent. It can be appreciated that in the MN11-275α extrusion, recrystallization is not fully completed, as a few large deformed grains elongated along the ED (see red arrows in Figure 2) are still present. In the remaining extrusions, the microstructure is completely recrystallized.

The average grain size of the MN11 alloy is, in general, very similar to that of the MN10 alloy for the same extrusion conditions. It can be also noted that the average grain size after extrusion in both alloys slightly increases with increasing extrusion temperature and speed, due to the faster diffusion rates and more prolonged cooling times.

It has been shown earlier[12] that, during extrusion, the actual processing temperature is different from the initial temperature. Indeed, the temperature increases during the first stages of the extrusion process and then remains constant. In addition, Bohlen et al.,[8] have shown that increasing the extrusion speed results in a higher temperature increment during the extrusion process and is, thus, equivalent to increasing the processing temperature which, in turn, leads to faster diffusion rates. It must also be mentioned that the dynamically recrystallized microstructures are not quenched after extrusion. During the cooling process, there can be enough heat to promote grain growth. So, higher extrusion temperature and speed not only increase the diffusion rate but also prolong the cooling time and thus the time for potential grain growth.[12]

Figure 3 illustrates the particle distribution in the MN11 alloy processed at 548 K (275 °C) and 2.8 mm/s and 350 °C and 11 mm/s. A close inspection of both extruded bars by SEM reveals that there is a bimodal particle size distribution in the Mg-Mn-Nd alloys after extrusion and cooling. The larger particles, with a mean size around 1 μm, contain Nd, while the smaller particles, with a mean size around 100 nm, contain Mn. Note that, considering that the dimension of the particles is beyond the resolution of the EDS probe, the concentration of Mg element is overestimated in both cases, especially in the Mn-containing particles. The comparison between both extruded bars one another reveals, additionally, that, while the Mn-containing particles are thermally stable, the amount of the particles containing Nd decreases with increasing the extrusion temperature and speed. This can be attributed to the considerable increase of solid solubility of system Mg-Nd with increasing temperature.[13]

The inverse pole figures (IPFs) in the ED of the MN10 extruded bars are shown in Figure 4. The typical prismatic $\langle 10\bar{1}0 \rangle$ fiber component dominates the texture of all the extruded bars. Furthermore, the extrusion axes tend to spread preferentially along an arc between the $\langle 10\bar{1}0 \rangle$ pole and an orientation along the $\langle 11\bar{2}0 \rangle$ to $\langle 0001 \rangle$ boundary, close to the $\langle 11\bar{2}0 \rangle$ pole, which has been directly related to the presence of the RE elements.[9] The width of the above-mentioned orientation arc is broader than that typical of extruded non-RE-containing alloys, such as M1 (Mg-1 wt pct Mn), where such arc lies between the $\langle 10\bar{1}0 \rangle$ and the $\langle 11\bar{2}0 \rangle$ poles. Thus, the extrusion texture of the MN10 alloy is generally weaker than that of the conventional Mg alloys.[8] The intensity of the $\langle 10\bar{1}0 \rangle$ peak increases with increasing extrusion temperature and speed. It is interesting to point out that the MN10-300α and β extrusions exhibit a weak, but significant, basal component in which the c-axes are parallel to the ED, so that the prismatic planes are parallel to the ED. This unusual component has been also recently observed by Robson et al.,[14] who claimed that it arises from recrystallized grains that have a growth advantage.

The IPFs in the ED of the MN11 extruded bars are shown in Figure 5. It can be seen that the MN11 alloy extruded bars exhibit a very broad angular distribution of the ED and thus a significant weaker texture than the MN10 extrusions. In some cases, the polycrystalline MN11 samples are nearly randomly oriented. The texture of the MN11 alloy consists, in general, of three main components, schematically depicted in the inset of Figure 5. The first one, indicated by a red curve and termed component A, is the orientation arc spreading from the $\langle 10\bar{1}0 \rangle$ pole toward the $\langle 11\bar{2}0 \rangle$ to $\langle 0001 \rangle$ boundary, which was reported above for the MN10 alloy as well as in previous reports on other RE-containing Mg alloys.[8,9,12,15,16] The second one has been named component B and is represented by means of a blue curve. It is another orientation arc spanning from the $\langle 11\bar{2}0 \rangle$ to $\langle 0001 \rangle$ boundary toward the $\langle 10\bar{1}0 \rangle$ to $\langle 0001 \rangle$ boundary. Finally, component C, indicated by a yellow area, corresponds to orientations for which the ED is close to the c-axes. The intensity of these components varies as a function of the extrusion conditions in the following way. In the samples processed at 548 K (275 °C), for the lowest extrusion speeds, the texture is formed by components A and B. Component C appears with increasing speed. In the samples processed at the highest temperature, i.e., 623 K (350 °C), for the lowest extrusion speeds, the texture is formed by components A and C and, with increasing speed, component C disappears. In summary, it is suggested by the authors that as extrusion temperature and speed increase, i.e., as the diffusion rate increases, the processing texture changes following the sequence A + B → A + B + C → A + C → A.

Overlaid tensile and compressive true stress–true strain (σ–ε) curves from the mechanical tests performed at 10^{-3} s^{-1} and room temperature on the specimens parallel to the ED are shown in Figures 6 and 7. The work hardening rate (θ) of every σ–ε curve until the strain level corresponding to the maximum stress is also plotted in the figures. Figure 8 gives the tensile and compressive yield stress values (σ_y) corresponding to the tests performed as a function of the extrusion temperature and speed. The two alloys exhibit a significantly different behavior. The shape of the curves corresponding to the MN10 alloy is concave down under tensile loading and concave up under compressive loading. Thus, θ of the tensile curves decreases with increasing ε, while θ of the compressive curves exhibits a maximum at an intermediate ε. This is consistent with the predominance, during the first deformation stages, of prismatic slip in tension and of $\{10\bar{1}2\}$ twinning in compression, as observed in non-RE-containing alloys, such as AZ31.[17] A yield stress asymmetry can be clearly seen. The tensile yield stress is similar for all the extrusion conditions (approximately 140 MPa). The compressive yield stress, which also remains largely constant with increasing extrusion speed, exhibits lower values than the tensile yield stress, especially in the extrusions processed at 633 K (360 °C), for which σ_y is approximately 100 MPa. The yield asymmetry is more prominent for the extrusions processed at 633 K (360 °C) than for those extruded at 573 K (300 °C) because they have sharper $\langle 10\bar{1}0 \rangle$ fiber textures (Figure 4), i.e., more grains are suitably oriented
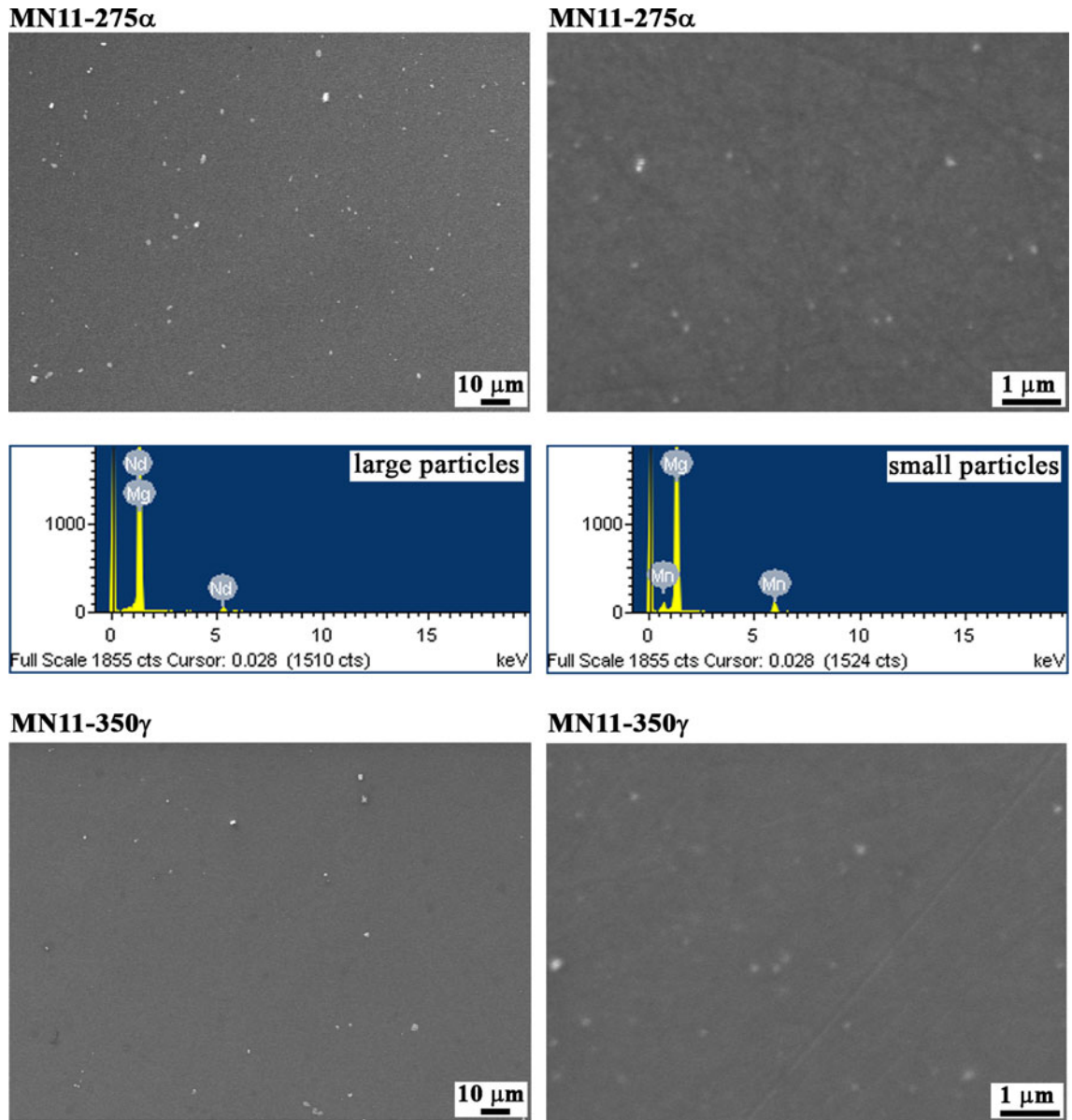
Fig. 3—SEM micrographs showing particles from the transversal section of the MN11-275α and the MN11-350γ extrusion bars and EDS results of the large and the small particles.

for twinning, leading to inferior compressive yield stresses (Figure 8). The increase of the yield asymmetry with increasing extrusion temperature is also related to the observed increase of the average grain size. This is consistent with previous studies.[18]

In the MN11 alloy, the yield stress asymmetry is significantly smaller than in the MN10 alloy and, in the samples extruded at 548 K (275 °C), it becomes negligible. σ_y values are observed to decrease with increasing extrusion speed from around 115 to 90 MPa. Moreover, the shape of the curves is similar in tension and compression, revealing that the same deformation mechanisms are activated under both testing conditions. This is particularly true for the extrusions carried out at 548 K (275 °C). Given that the MN11 alloy exhibits very weak extrusion textures (most noticeably in the

MN11-275γ sample), basal slip should be the dominant deformation mechanism irrespective of the testing mode. Therefore, concave down-shaped curves would be expected for such alloy in both tensile and compressive tests along the ED. However, the presence of a maximum in all the θ vs. ε curves reveals an anomalously large twinning activity during the first stages of deformation, both in tension and in compression along the ED.

IV. DISCUSSION

A. Effect of Nd Content on Texture Development

The present results demonstrate that irrespective of the Nd content, the grain size of the two alloys investigated is, for the same extrusion conditions, very similar. Small
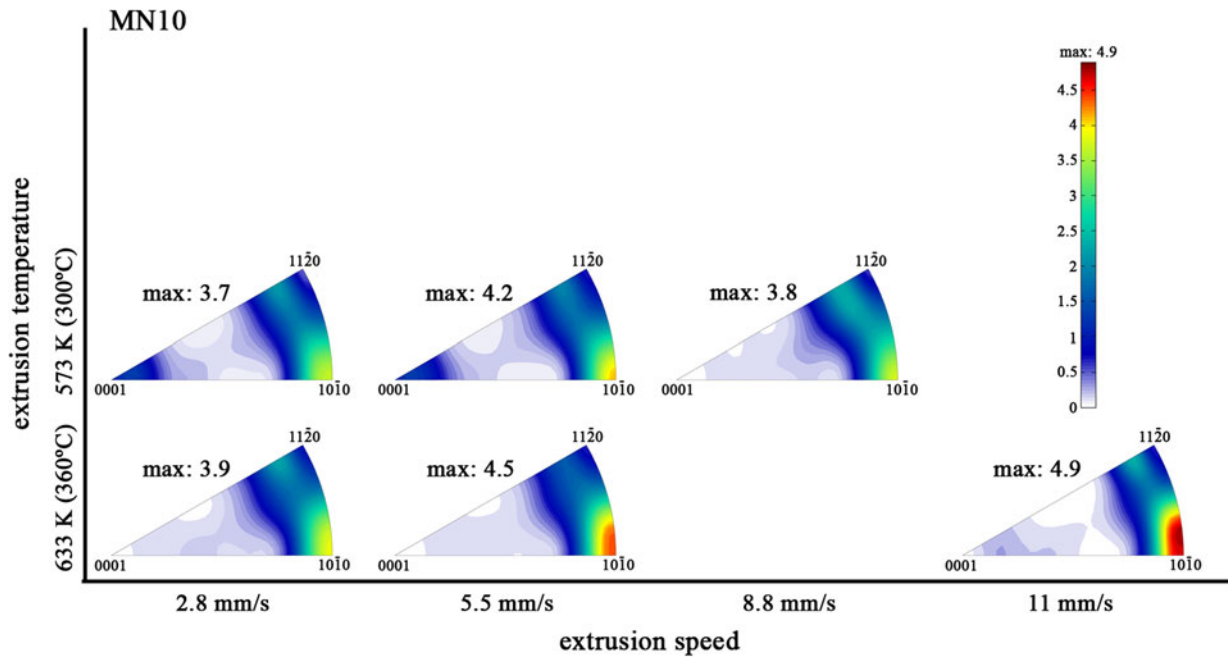
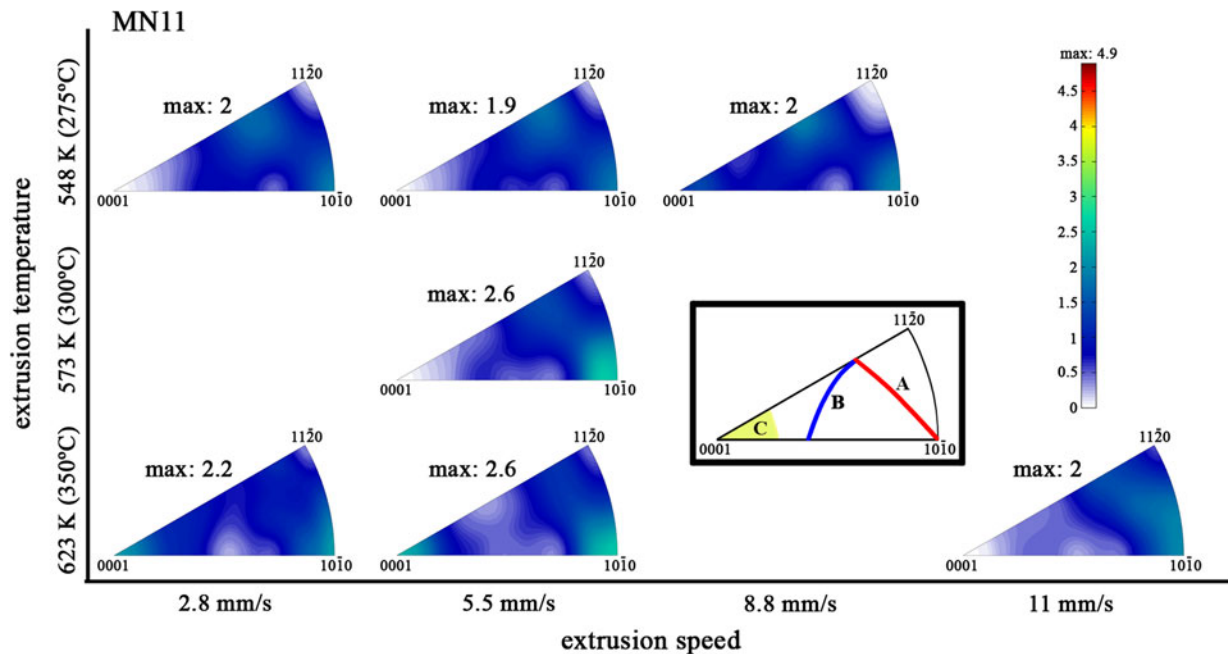Fig. 4—Inverse pole figures in the ED of the MN10 bars.

Fig. 5—Inverse pole figures in the ED of the MN11 bars. A schematic figure showing the three main components composing the extrusion texture of the MN11 is also included.

size changes are only noticeable when the extrusion temperature and speed increase. We propose that in these alloys the grain size may be controlled by the presence of the Mn-containing particles, which due to their small mean size, would exert a strong pinning force on grain boundaries.[19] The increment of the average grain size with increasing extrusion temperature and speed could be attributed to the increase of the boundary mobility with temperature, which would result in a smaller efficiency of particle pinning. Given that the amount of

Mn is identical in the MN10 alloy and in the MN11 alloy and that the particles containing Mn are essentially thermally stable, the pinning effect of such particles could explain the similarity of the average grain sizes in both alloys, but not the weak textures of the MN11 extrusions relating to those of the MN10 extrusions.

The present results also prove that increasing the content of Nd results in a decrease of the texture strength and in the appearance of new texture components, in which the extrusion axis has an orientation that
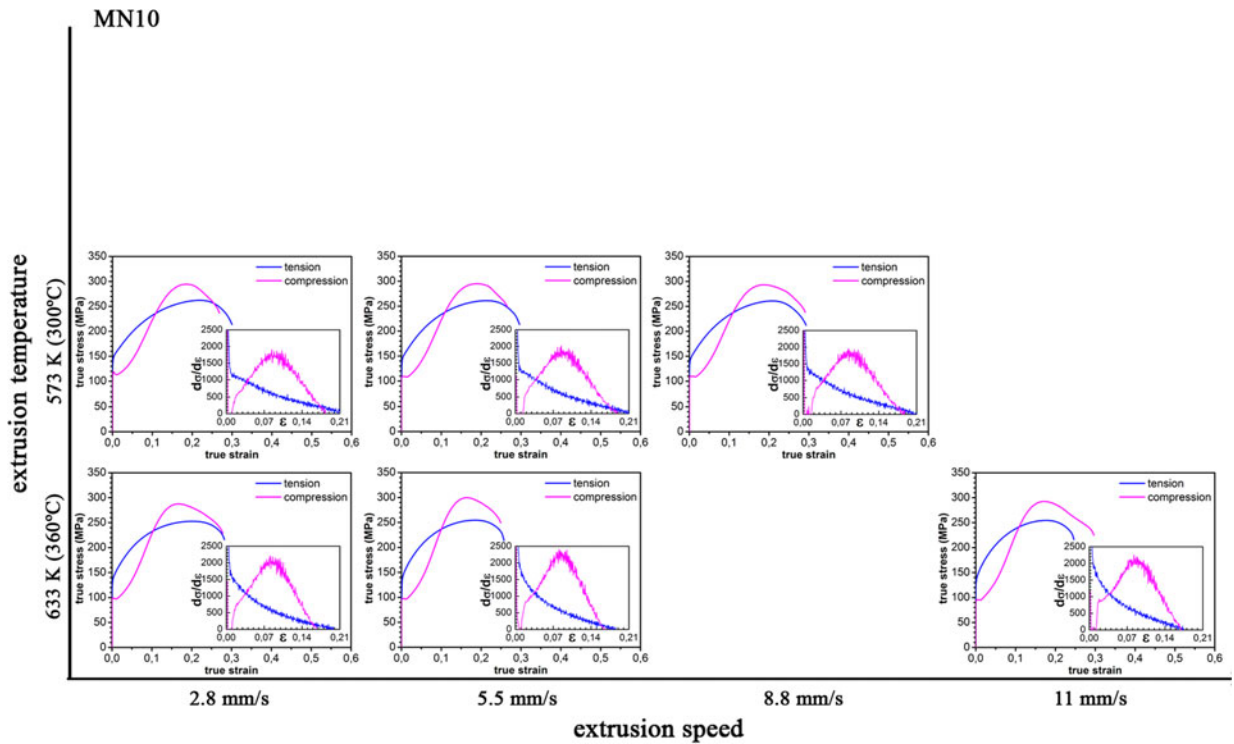
Fig. 6—Tensile and compressive true stress (σ)–true strain (ε) curves and the work hardening rate ($\theta = d\sigma/d\varepsilon$) corresponding to the tests performed at 10^{-3} s^{-1} and room temperature on the MN10 bars along the ED.

Fig. 7—Tensile and compressive true stress (σ)–true strain (ε) curves and the work hardening rate ($\theta = d\sigma/d\varepsilon$) corresponding to the tests performed at 10^{-3} s^{-1} and room temperature on the MN11 bars along the ED.
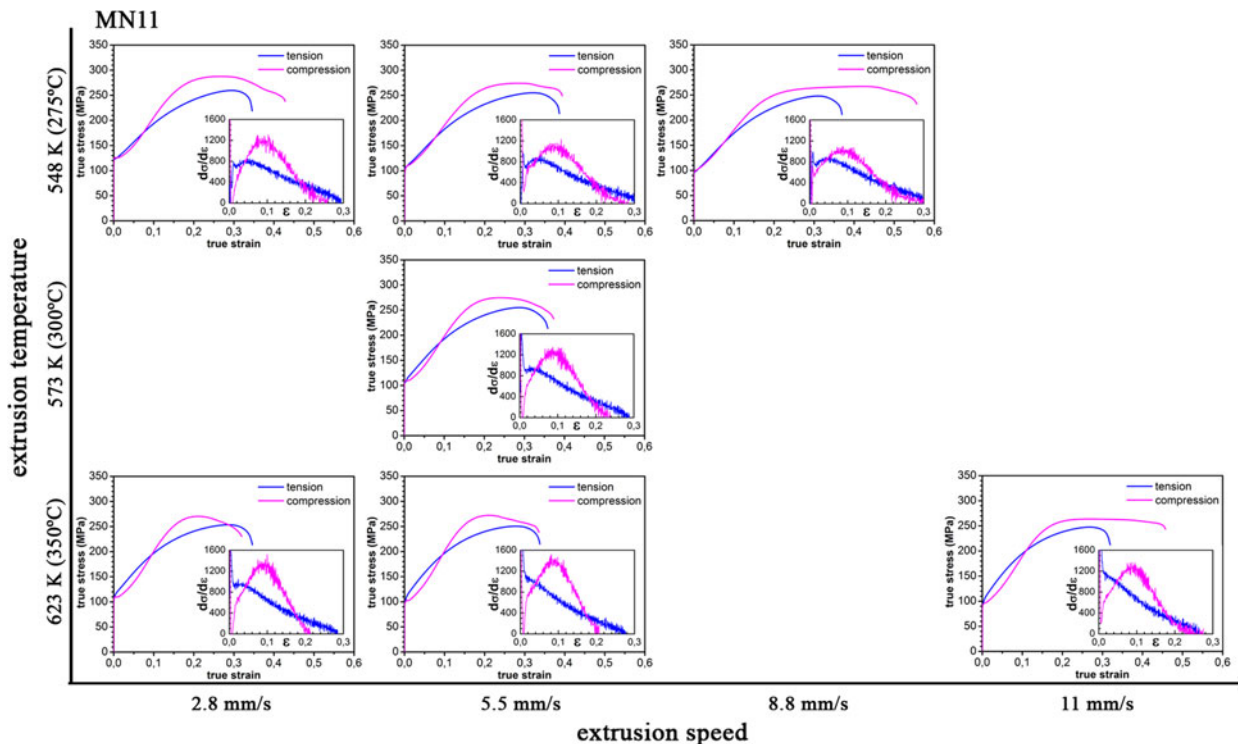
is tilted away from the $\langle 10\bar{1}0 \rangle$ to $\langle 11\bar{2}0 \rangle$ boundary of the stereographic triangle. This is consistent with previous studies on RE-containing alloys, which often exhibit rather weak textures after wrought processing compared to the conventional Mg alloys.[2,6–9,16,20–23] The origin of this unusual texture development is still not clear. The
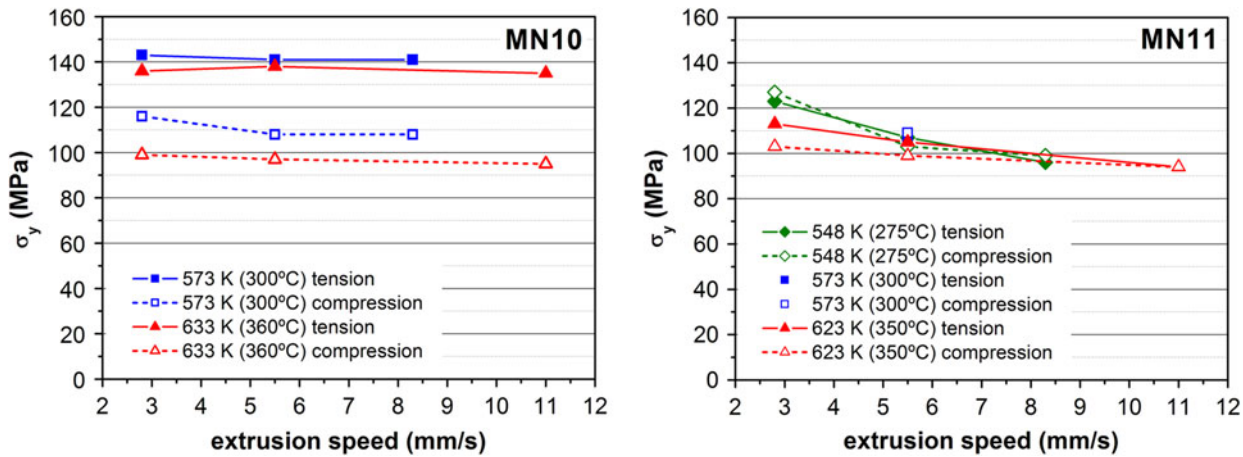
Fig. 8—Variation of the tensile and compressive yield stress (σ_y) corresponding to the tests performed at 10^{-3} s^{-1} and room temperature on the MN10 and the MN11 bars with the extrusion temperature and speed.

following explanations have been put forward by different authors.

In an earlier study[6] on the texture of the extruded WE54 (Mg-5.2Y-1.74Nd-0.95RE-0.59 wt pct Zr) alloy, the texture weakening observed was attributed to a PSN mechanism. In that case, the material was highly alloyed and contained coarse particles, which favored the formation of local deformation zones, where nucleation of randomly oriented grains took place preferentially. A later work[7] confirmed that PSN contributes to the development of a weaker texture during extrusion of the WE43 (Mg-3.88Y-2.26Nd-0.80Zr-0.10La-0.08 wt pct Pr) alloy. However, it was found that this mechanism was not fully responsible for the final texture since the grains formed in the vicinity of particles are not able to compete with those formed at other sites. Thus, it is unlikely that the recrystallization of the alloys in this study, which have smaller concentrations of RE elements, is dominated by PSN. Moreover, it has been shown in[2] that the presence of solute RE elements alone (in solid solution, without particles) is sufficient to produce a change in the texture in RE-containing Mg alloys without invoking PSN. Another possible mechanism put forward for the weakening of the texture and for the formation of unusual texture components is a higher propensity for oriented nucleation at shear bands in the RE-containing alloys.[9] Conventional Mg alloys also exhibit shear banding during extrusion, but nucleation of new grains has been observed to take place preferentially within the homogeneously deformed regions (i.e., outside shear bands) giving rise to the typical extrusion texture in which the orientation of the ED clusters around the $\langle 10\bar{1}0 \rangle$ to $\langle 11\bar{2}0 \rangle$ boundary of the stereographic triangle. Finally, retardation of grain growth could also result in weak textures in fully recrystallized materials.[8] A mechanism involving particle pinning can be considered to restrict the preferential growth of certain orientations and thus enable grains with other orientations to grow.

Due to the presence of the fine Mn-containing particles, alteration of the texture by restricted grain growth due to particle pinning seems to be a plausible mechanism that could be responsible for the weak textures measured in the Mg-Mn-Nd alloys, at least at the lowest extrusion temperatures and speeds. It has been proposed[8] that particles may pin the grain boundaries leading to a weakening of the texture and to the stabilization of unusual components. Since, in the two alloys investigated, the grain sizes are similar but the strength of the texture is highly dependent on the Nd content, we propose that the addition of a higher amount of Nd could additionally result in the nucleation of grains with a wider range of orientations during hot extrusion.[8] As the extrusion temperature and speed increase, grain growth is less restricted and orientations that are more similar to those of conventional extruded Mg alloys develop. Mackenzie and Pekguleryuz[21] found that the presence of shear bands, and thus the frequency of nucleation in the shear band interiors, is higher in the Mg-RE alloys than in the non-RE Mg alloys. This effect could be more important with increasing the RE content.

B. Oriented Nucleation and Oriented Growth in Nd-containing Mg Alloys

The examination of the MN11 extrusion textures and microstructures (Figures 2 and 5) gives valuable information about the kinetics of texture development in Nd-containing Mg alloys. In the MN11-275α extrusion, the texture is formed by the A and B "orientation arcs." In this sample, the process of recrystallization was found to be incomplete as some original grains, elongated along ED, remain present after the processing. With increasing extrusion speed at the same temperature, the microstructure becomes fully recrystallized and simultaneously a depletion of intensities in the vicinity of the $\langle 11\bar{2}0 \rangle$ pole and the appearance of the basal component (C) are observed. This suggests that grains in which the ED is close to the $\langle 11\bar{2}0 \rangle$ direction are those with the highest resistance to recrystallization and those with basal orientations are the last ones to be nucleated during extrusion. These orientation changes lead to the stabilization of a nearly random texture in the MN11-275γ alloy.

As the extrusion temperature and speed increase, grain growth of selected orientations takes place. A close look at the evolution of the texture of the MN11 samples extruded at 623 K (350 °C) with increasing speed reveals that the first orientations to be consumed are those belonging to the B component and then those belonging to the C component. Thus, at the highest extrusion speed (MN11-350γ), the texture is formed exclusively by the A component, *i.e.*, the fiber between the $\langle 10\bar{1}0 \rangle$ and the so-called RE component (an orientation along the $\langle 10\bar{1}0 \rangle$ to $\langle 11\bar{2}0 \rangle$ boundary, close to the $\langle 11\bar{2}0 \rangle$ pole). In the MN10 alloy, orientation selection by grain growth takes place at comparatively lower temperatures. Thus, in the MN10 alloy at 633 K (360 °C), only the A component remains, irrespective of the extrusion speed. Moreover, at the the highest extrusion speed, the $\langle 10\bar{1}0 \rangle$ prismatic fiber develops a higher growth advantage and the A component shifts toward the $\langle 10\bar{1}0 \rangle$ to $\langle 11\bar{2}0 \rangle$ boundary of the stereographic triangle. This last observation seems to be consistent with the findings made by Stanford and Barnett,[9] according to which there is a stepwise change in the texture from one with an outstanding RE component at low temperatures to a more conventional extrusion texture at higher temperatures. It is expected that in both, the MN10 and MN11 alloy, processing at still higher temperatures and extrusion speeds would ultimately lead to the texture of conventional extruded Mg alloys.

C. *Effect of Nd on the Critical Resolved Shear Stress of Basal Slip (CRSS$_{basal}$)*

Our results suggest an anomalously high activity of tensile twinning during room temperature deformation in tension and in compression of the MN11 extrusions, particularly in those processed at the lowest temperature, *i.e.*, 548 K (275 °C), which have nearly random textures. This observation can be rationalized as follows. Basal slip is usually the most easily activated mechanism in Mg alloys due to its reduced critical resolved shear stress (CRSS). However, basal slip systems can be significantly strengthened by precipitates.[24] An increase in the CRSS of basal slip (CRSS$_{basal}$) in a randomly (or nearly randomly) oriented Mg polycrystal would alter the relative activities of basal slip and extension twinning, enhancing that of the latter. According to the analysis made by Nie,[25] the precipitate shape and orientation are the major factors affecting the strengthening of age-hardenable Mg alloys. Nie[25] suggests that plates on prismatic planes have the most effective geometry and orientation for impeding basal slip. This is because the probability of such plates being intersected by a given basal plane is very high, leading to a little interparticle spacing on the plane.

In the Nd-containing Mg alloys, four aging stages have been described: supersaturated solid solution (SSSS) $\rightarrow$ Guinier–Preston (GP) zones (MgNd) $\rightarrow$ β'' (Mg$_3$Nd, DO$_{19}$, coherent) $\rightarrow$ β' (Mg$_3$Nd, hexagonal, semi-coherent) $\rightarrow$ β (Mg$_{12}$Nd, bct, incoherent).[1,13] The
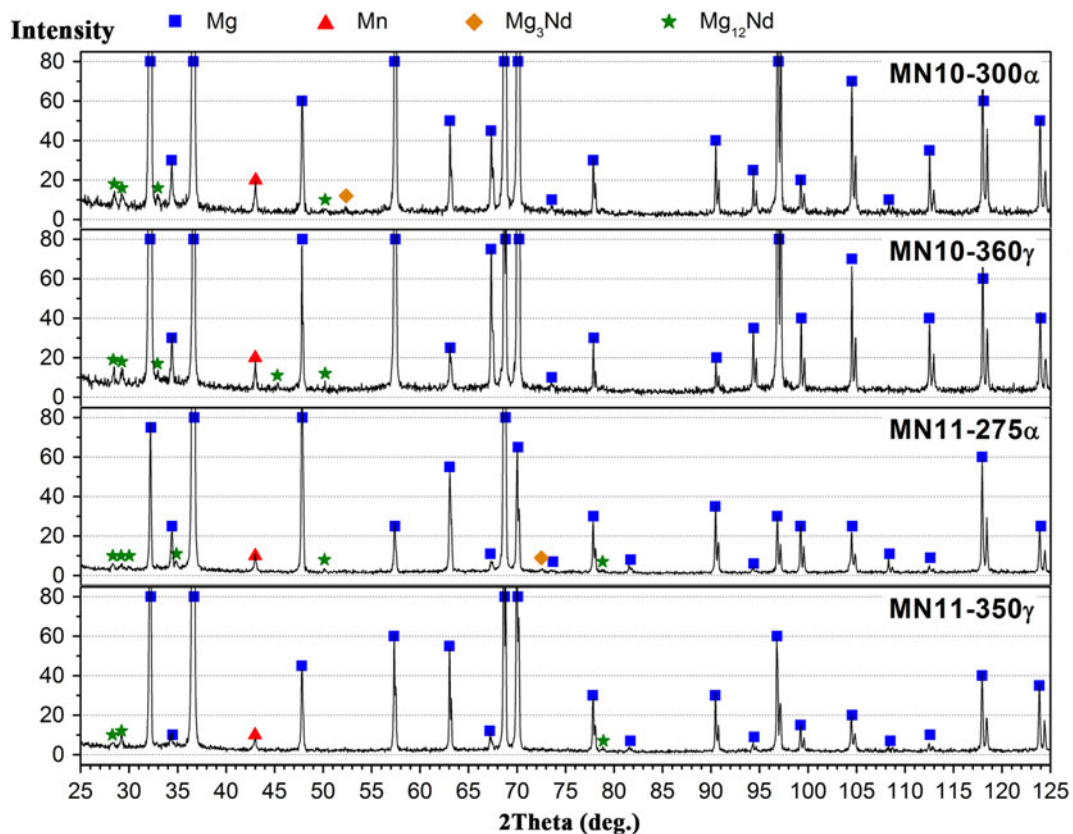
Fig. 9—XRD patterns of the MN10-300α, MN10-360γ, MN11-275α, and MN11-350γ extrusion bars.

β'' and β'-phases are plates along prismatic planes that are nucleated when the alloys are aged at temperatures ranging approximately from 473 K (200 °C) to 573 K (300 °C). Above this range, they are superseded by the equilibrium β-phase, which is irregularly shaped and thus is not as effective as β'' and β'-phases for impeding slide in the basal planes. So, the presence of Mg_3Nd could result in an increase in the CRSS of basal slip in our Mg-Mn-Nd alloys. Our results showed, indeed, that relatively large Nd-containing particles were present in the MN11 alloy extruded at low temperatures and speeds and that the amount of such particles decreased significantly as the temperature and speed increased. Furthermore, the XRD patterns of Figure 9 show that both the Mg_3Nd and the $Mg_{12}Nd$ phases are present in the MN10-300α and the MN11-275α extruded bars, while in the MN10-360γ and the MN11-350γ samples, only the presence of $Mg_{12}Nd$ phase is noticeable. The XRD patterns of Figure 9 also reveal that the Mn-containing particles are close to pure Mn in composition. The presence of intermetallic prismatic plates in the extruded microstructures, especially at low extrusion temperatures and speeds, would lead to a significant strengthening of basal slip, especially in the MN11 samples and, in turn, to the enhanced activation of twinning observed. This observation is in agreement with the lower yield stress asymmetry in the MN11 samples extruded at 548 K (275 °C). Also, both the dissolution of the Nd-containing particles and the gradual transformation of the Mg_3Nd phase into the $Mg_{12}Nd$ phase would be consistent with the increasingly lower activation of twinning with increasing extrusion temperature and speed. On the other hand, since the content of Nd is higher in the MN11 alloy than in the MN10 alloy, a higher amount of Mg-Nd precipitates, including those corresponding to the Mg_3Nd phases, is expected. This, together with the fact that the textures are stronger in the MN10 alloy, would explain the larger yield asymmetry in this material.

The alteration of the CRSS of non-basal slip systems by the addition of RE elements has been previously reported by several authors.[14,23,26,27] The origin of the increased non-basal activity is still not clear. Chino et al.[22,26] and Sandlöbes et al.[27] suggested that the stacking fault energies of certain types of dislocations changed by the addition of Ce and Y, respectively, thus altering the CRSS of $\langle a \rangle$ and $\langle c + a \rangle$ slip. Robson et al.[14] carried out VPSC modeling to simulate the behavior of a Mg-6Y-7Gd-0.5 wt pct Zr alloy and found that the best fit was obtained when the relative CRSS of prismatic slip was significantly reduced with respect to that of a conventional alloy such as AZ31. Our results suggest, furthermore, that RE elements influence significantly the $CRSS_{basal}$. As the extrusion temperature increases, two phenomena take place simultaneously. On the one hand, the dissolution of the Nd-containing particles and the transformation of the Mg_3Nd phases into the $Mg_{12}Nd$ phase occurs, which would lead to a decrease of the $CRSS_{basal}$. On the other hand, boundary pinning by particles is reduced, resulting in textures formed mainly by the A component. Thus, different deformation mechanisms operate in tension and in compression. This justifies the differences in the shape of the compressive and tensile curves observed in, for example, the MN11-350β and γ samples (Figure 6).

It has been demonstrated that the shape and the orientation of precipitates have a critical influence in the strengthening of different deformation modes in Mg-Mn-Nd alloys. The fact that this effect favorably alters the balance in strength of various deformation modes is of great technological interest. In particular, our work provides further evidence that careful design of precipitation processes by tuning the alloy composition and the thermal treatment might prove to be a useful tool for reducing the asymmetry in wrought Mg alloys.[28]

V. CONCLUSIONS

A Mg-1 wt pct Mn alloy containing 0.5 wt pct Nd (MN10) and 1 wt pct Nd (MN11) was extruded at temperatures ranging from 548 K (275 °C) to 633 K (360 °C) and speeds between 2.8 and 11 mm/s. A total of 13 different extrusion conditions are included in the present study. The microstructure, the texture, and the room temperature mechanical behavior of all the extrusions were analyzed in order to investigate the effect of the processing conditions and of the Nd content on the selection of orientations during processing as well as on the predominant deformation mechanisms. The following conclusions have been obtained from the present study:

1. The microstructures of the extruded samples are in general fully recrystallized. Only the MN11 alloy extruded at the lowest temperature and speed exhibits some deformed grains, elongated along the ED. The particle distribution in the Mg-Mn-Nd alloys investigated is bimodal. In particular, fine Mn-containing particles, about 100 nm in size, and coarser Nd-containing particles, about 1 μm in size, are present.

2. The small Mn-containing particles, which are thermally stable, are proposed to be responsible for pinning of grain boundaries, leading to the development of similar grain sizes in both alloys for the same extrusion conditions. The average grain size slightly increases with increasing extrusion temperature and speed due to a smaller efficiency of particle pinning.

3. Increasing the amount of Nd gives rise to significant weakening of the extrusion textures. This may be a consequence of the nucleation of a wider range of orientations as Nd content increases.

4. Additions of 1 wt pct of Nd lead to the disappearance of the yield asymmetry at room temperature and to tensile and compressive stress vs strain curves with very similar concave up shapes, especially at the lowest extrusion temperatures. This suggests an anomalously high activity of tensile twinning, which is attributed to an increase in the critical resolved shear stress of basal slip due to the presence of Mg_3Nd coherent and semi-coherent intermetallic plates along prismatic planes.

5. At the highest extrusion temperatures investigated, the extrusion textures and the mechanical behavior in tension and in compression tend toward those of

conventional extruded Mg alloys, especially in the samples with lower Nd content. This is attributed to less effective particle pinning of grain boundaries as well as to a limited effect of the RE elements on the critical resolved shear stress of basal slip due to the dissolution at these temperatures of the Mg_3Nd particles.

ACKNOWLEDGMENTS

REFERENCES

1. I.J. Polmear: *Light Alloys. Metallurgy of the Light Metals*, 2nd ed., Edward Arnold, London, 1989, pp. 169–10.
2. J. Bohlen, M.R. Nürnberg, J.W. Senn, D. Letzig, and S.R. Agnew: *Acta Mater.*, 2007, vol. 55, pp. 2101–12.
3. I.L. Dillamore and W.T. Roberts: *Metall. Rev.*, 1965, vol. 10, pp. 271–80.
4. J.W. Christian and S. Mahajan: *Prog. Mater. Sci.*, 1995, vol. 39, pp. 1–157.
5. M.R. Barnett: *Mater. Sci. Eng. A*, 2007, vol. 464A, pp. 1–7.
6. E.A. Ball and P.B. Prangnell: *Scripta Metall. Mater.*, 1994, vol. 31, pp. 111–16.
7. L.W.F. Mackenzie, B. Davis, F.J. Humphreys, and G.W. Lorimer: *Mater. Sci. Technol.*, 2007, vol. 23, pp. 1173–80.
8. J. Bohlen, S. Yi, D. Letzig, and K.U. Kainer: *Mater. Sci. Eng. A*, 2010, vol. 527A, pp. 7092–98.
9. N. Stanford and M.R. Barnett: *Mater. Sci. Eng. A*, 2008, vol. 496A, pp. 399–08.
10. M.O. Pekguleriuz: in *Advances in Wrought Magnesium Alloys. Fundamentals of Processing, Properties and Applications, 1st ed.*, Woodhead Publishing Limited, Cambridge, 2012, pp. 3–62.
11. J.D. Robson, D.T. Henry, and B. Davis: *Mater. Sci. Eng. A*, 2011, vol. 528A, pp. 4239–47.
12. T. Laser, Ch. Hartig, M.R. Nürnberg, D. Letzig, and R. Bormann: *Acta Mater.*, 2008, vol. 56, pp. 2791–98.
13. T.J. Pike and B. Noble: *J. Less-Common Met.*, 1973, vol. 30, pp. 63–74.
14. J.D. Robson, A.M. Twier, G.W. Lorimer, and P. Rogers: *Mater. Sci. Eng. A*, 2011, vol. 528A, pp. 7247–56.
15. J. Bohlen, S.B. Yi, J. Swiostek, D. Letzig, H.G. Brokmeier, and K.U. Kainer: *Scripta Mater.*, 2005, vol. 53, pp. 259–64.
16. N. Stanford, D. Atwell, A. Beer, C. Davis, and M.R. Barnett: *Scripta Mater.*, 2008, vol. 59, pp. 772–75.
17. I.Ulacia, N.V. Dudamell, F. Gálvez, S. Yi, M.T. Pérez-Prado, and I. Hurtado: *Acta Mater.*, 2010, vol. 58, pp. 2988–98.
18. J. Bohlen, P. Dobroň, J. Swiostek, D. Letzig, F. Chmelík P. Lukáč, and K.U. Kainer: *Mater. Sci. Eng. A*, 2007, vol. 462A, pp. 302–06.
19. C. Zener: quoted by C.S. Smith: *Trans. Metall. Soc. A.I.M.E.*, 1948, vol. 175, pp. 15–51.
20. N. Stanford and M. Barnett: *Scripta Mater.*, 2008, vol. 58, pp. 179–82.
21. L.W.F. Mackenzie and M.O. Pekguleryuz: *Scripta Mater.*, 2008, vol. 59, pp. 665–68.
22. Y. Chino, M. Kado, and M. Mabuchi: *Mater. Sci. Eng. A*, 2008, vol. 486A, pp. 343–49.
23. K. Hantzsche, J. Bohlen, J. Wendt, K.U. Kainer, S.B. Yi D. Letzig: *Scripta Mater.*, 2010, vol. 63, pp. 725–30.
24. S.R. Agnew: in *Advances in Wrought Magnesium Alloys. Fundamentals of Processing, Properties and Applications*, 1st ed., Woodhead Publishing Limited, Cambridge, 2012, pp. 63–104.
25. J.F. Nie: *Scripta Mater.*, 2003, vol. 48, pp. 1009–15.
26. Y. Chino, M. Kado, and M. Mabuchi: *Acta Mater.*, 2008, vol. 56, pp. 387–94.
27. S. Sandlöbes, S. Zaefferer, I. Schestakow, S. Yi, and R. Gonzalez-Martinez: *Acta Mater.*, 2011, vol. 59, pp. 429–439.
28. J.D. Robson, N. Stanford, and M.R. Barnett: *Acta Mater.*, 2011, vol. 59, pp. 1945–56.